A Multitemporal Investigation of AMSR-E C-Band Radio-Frequency Interference

Teodosio Lacava, *Member, IEEE*, Irina Coviello, Mariapia Faruolo, Giuseppe Mazzeo, Nicola Pergola, *Member, IEEE*, and Valerio Tramutoli

***Abstract*—Radio-frequency interference (RFI) is increasingly a severe problem for present and future microwave satellite missions. RFI at C- and X-bands can contaminate remotely sensed measurements, as experienced with the Advanced Microwave Scanning Radiometer (AMSR-E) and the WindSat sensor. In this work, the multitemporal Robust Satellite Techniques approach has been implemented on C-band AMSR-E data in order to identify areas systematically affected by different levels of RFI, trying to discriminate them from natural geophysical variability zones. To the scope, nine years of AMSR-E data have been investigated, allowing us also to better infer RFI impact on data acquired during ascending or descending passes, as well as in horizontal or vertical polarization. In detail, two analyses were carried out: one considering only measurements at C-band and another one taking into account a combination between C- and X-band measurements. The results of this study will be shown and discussed in this paper.**

***Index Terms*—Advanced Microwave Scanning Radiometer (AMSR-E), passive microwave remote sensing, radio-frequency interference (RFI), Robust Satellite Techniques (RST).**

I. Introduction

OVER the last several years, the problem of radio-frequency interference (RFI) in spaceborne microwave radiometer data has seriously impacted remote-sensing science products. Such a trend is expected to increasingly rise in the next years because the frequency requirements of remote sensing have begun to overlap active radio service allocations [1]. In detail, RFI is often caused by manmade emission sources such as telecommunication transmissions, civilian and military radars, high-bandwidth point-to-point terrestrial wireless communication links, and wireless routers [2], [3]. Also, unwanted high emissions of active service stations operating at bands adjacent to the protected ones may produce RFI [4]. Recent experiences with passive microwave sensors, like the Advanced Microwave Scanning Radiometer (AMSR-E) aboard the Earth Observing System Aqua platform and the WindSat radiometer on the U.S. Department of Defense Coriolis satellite, both working at low microwave frequencies of the electromagnetic spectrum, have demonstrated the increasing RFI impact on the measured signal and its effect on geophysical parameter retrieval [5]–[10]. Indeed, in addition to data acquired at C-band (6.7–7.1 GHz for AMSR-E and 6.74–6.86 GHz for WindSat), X-band (10.6–10.7 GHz for AMSR-E and 10.55–10.85 GHz for WindSat) data, although they are acquired at a protected band [11], have been discovered to be affected by RFI contamination. It should be stressed that AMSR-E uses, at X-band, a bandwidth of 100 MHz which is larger than the protected one (10.6–10.68 GHz), so that it is also sensitive to borderline but authorized emissions. RFI impact on received data has been further confirmed by the first data acquired at L-band (1.40–1.427 GHz) by the Microwave Imaging Radiometer with Aperture Synthesis aboard the European Space Agency/Soil Moisture and Ocean Salinity mission, where large areas of the world have been discovered to be RFI affected also at these protected wavelengths [4], [12]–[18]. If not properly identified and rejected, RFI contamination could significantly reduce the science value of existing and future C- and X-band passive microwave missions [8], [10], [19], like the Advanced Microwave Scanning Radiometer 2 (AMSRE-2) aboard the Japanese Shizuku mission (originally Global Change Observation Mission 1st—Water) [20] launched on May 18, 2012 [21], as well as the L-band microwave missions, like NASA AQUARIUS [22], [23] launched in June 2011 and Soil Moisture Active–Passive [24] scheduled for November 2014.

Thus, if for future missions, RFI detection and mitigation strategies are needed to ensure that radiometer measurements will not be damaged by extreme RFI, for past data, it is fundamental to develop new suitable and reliable data postprocessing strategies [1], [25] in order to reduce the impact of RFI on the measured signal at the sensor.

Several authors have already investigated AMSR-E and WindSat C- and X- band RFI [5]–[10]. One still open issue is the reliable identification of areas where low levels of RFI are present and, therefore, the need of discriminating RFI-affected areas from zones having a high natural geophysical variability, such as those characterized by the presence of melting ice or seasonal vegetation trend. Considering that RFI is inherently a positive bias to observed brightness temperature (TB), low levels of RFI are probably the most of concern at least for long-term investigations, such as long-term climatological measurements [26].

In this work, the Robust Satellite Techniques (RST) approach [27], [28] has been implemented using AMSR-E C-band data to identify RFI source locations over land at global scale. In

Manuscript received February 28, 2012; revised September 20, 2012; accepted October 28, 2012.

T. Lacava, I. Coviello, M. Faruolo, G. Mazzeo, and N. Pergola are with the Institute of Methodologies for Environmental Analysis, National Research Council, 85050 Tito Scalo (PZ), Italy (e-mail: teodosio.lacava@imaa.cnr.it; irina.coviello@imaa.cnr.it; mariapia.faruolo@imaa.cnr.it; giuseppe.mazzeo@imaa.cnr.it; nicola.pergola@imaa.cnr.it).

V. Tramutoli is with the University of Basilicata, 85100 Potenza, Italy (e-mail: valerio.tramutoli@unibas.it).

Color versions of one or more of the figures in this paper are available online at http://ieeexplore.ieee.org.

Digital Object Identifier 10.1109/TGRS.2012.2228487

particular, such a study was aimed at identifying different levels of RFI contamination, trying to discriminate where natural (i.e., not RFI induced) geophysical variability is present. The RST approach has already demonstrated to be a suitable tool for monitoring many natural and environmental risks [27], [28], and the references herein also use AMSR-E data [29]–[31]. In addition, this original methodology, based on a multitemporal analysis of satellite records, colocated in the space–time domain, has already demonstrated to be able to reduce the impact of spurious contributes, known or not, (as those possibly caused by RFI) on the measured signals [32].

RST implementation on AMSR-E data will be presented in Section II, while the results of this analysis will be shown and discussed in Sections III and IV. Among its potential uses, the indication about RFI presence may be useful to localize where AMSR-E C-band data have to be used with attention in retrieving information about surface parameters (i.e., soil moisture and vegetation water content). In addition, such information could be used also during the early phase of the next AMSRE-2 to evaluate its effectiveness in overcoming AMSR-E RFI drawbacks.

II. Methodology

Passive microwave sensors measure the natural emission of energy from the Earth's surface. Considering AMSR-E low-frequency channels, the amount of the received microwave radiation depends on the emission and scattering at the surface [5], [7], [9], [10]. Over lands, these two parameters are functions of soil moisture, surface temperature, roughness, and vegetation cover. At C-band, water bodies show TBs of about 70 K with horizontal polarization and around 170 K with vertical polarization [10]. Land surfaces, having emissivities higher than water, show TBs in the range of 250 K–320 K, with a lesser but still present polarization difference [9], [10]. At X-band, the radiometric response of two surfaces (i.e., water and land) is similar to that at C-band even if, due to the spectral dielectric properties of soil and water mixture, TB at X-band is higher than the one measured at C-band for each surface. Considering that below 30-GHz scattering effects, whose increase may reduce TB relative variations [5], [7], are usually limited (except for dry snow, ice, and some desert surfaces), the natural positive spectral gradient between C- and X-band TBs may invert only in the presence of RFI [5], [7], [10]. To better evaluate C-band AMSR-E RFI contamination, an index based on the difference between measurements (in terms of TB) achieved for the same polarization (p = H or V) at 6.9 and 10.7 GHz has been proposed [5]

$$RI6.9p = TB6.9p - TB10.7p. \tag{1}$$

Positive values of such an index should indicate RFI presence. In particular, $5\ \text{K} < \text{RI6.9p} < 10\ \text{K}$ contains moderate RFI, while $\text{RI6.9p} > 10\ \text{K}$ contains strong RFI [5], [7]. In detail, in their analyses, Njoku *et al.* [7] used one year (June 2002–May 2003) of AMSR-E Level 2A data, concluding that a better characterization of RFI could have been obtained using classification thresholds varying spatially and temporally.

Starting from these considerations, we first applied the RST approach to the signal measured by AMSR-E at C-band (i.e., TB6.9p) and then to the index defined in (1) (i.e., RI6.9p). RST is an automatic change-detection scheme that identifies signal anomalies in the space–time domain as deviations from a normal state that has been preliminarily identified, at pixel level, on the basis of satellite observations collected during several years in the past, under similar observational conditions. By such an analysis, areas where the analyzed signal shows high persistent values in the space–time domain as well as high variability related to spurious and random effects such as those associated to radio interference effect should be easily highlighted.

In detail, AMSR-E Level-3 land surface product (AE_Land3) data [33] from June 2002 to May 2011 were used. The used gridded Level-3 land surface product includes daily measurements (stratified in ascending and descending passes) of surface soil moisture and vegetation/roughness water content interpretive information as well as TBs and quality control variables. Input TB data (both in horizontal and vertical polarizations), corresponding to a 56-km mean spatial-resolution image, are resampled to a global cylindrical 25-km Equal-Area Scalable Earth Grid cell spacing.

According to RST prescriptions, we computed, for each land pixel of such a grid, the temporal mean and the standard deviation of the TB6.9p and RI6.9p indexes for each of the 12 calendar months of the year. Specifically, the procedure we applied can be summarized as follows: 1) As a first step, all the AMSR-E data acquired for every calendar month were collected together (i.e., for the first month: January 2003, January 2004,. . . , January 2011, for the second: February 2003, February 2004,. . . , February 2011; and so on), stratifying them on the basis of their orbit type (i.e., ascending or descending) and polarization (i.e., horizontal or vertical); 2) then, for each of these 48 datasets (i.e., two polarizations + two orbit types for each calendar month), the temporal multiyear mean and standard deviation of the TB6.9p and RI6.9p indexes were computed. More than 3200 AMSR-E data ($\sim$96% of the whole AMSR-E dataset) have been processed to this scope; each calendar month dataset was composed of about 270 imagery. Such "reference fields" are used in this study to try to achieve a wide and clear view of RFI over land on a global scale. Areas where the analyzed signal showed high variability and/or persistent high values, both in intensity and time, should be, in fact, related to the presence of RFI [7]. We expect, in fact, that anthropogenic noise, as RFIs, appear stable in the space and time domains, whereas natural (e.g., geophysical and/or meteorological) processes are likely to occur with peculiar seasonality and/or periodicity. Reference fields should then be able to "synthesize" such a differential behavior, allowing for an effective discrimination of RFIs, although some considerations about possible limitations have to be done. Possible interannual changes, which may occur particularly because of geophysical/meteorological processes (e.g., snow/ice melting or the monsoon seasons) which may anticipate (or posticipate) their occurrence, from one year to another, should be taken into account. They may slightly modify statistics even if, working with sufficiently long (i.e., monthly) temporal windows, the

TABLE I
SUMMARY OF MONTHLY VALUES (IN KELVIN) OBTAINED BY AVERAGING OVER LAND-PIXEL RST MEAN TEMPORAL ESTIMATIONS ACHIEVED BY ANALYZING NINE YEARS OF AMSR-E C-BAND (TB6.9) MEASUREMENTS

	Mean-TB6.9_H_Des			Mean-TB6.9_H_Asc			Mean-TBI6.9_V_Des			Mean-TBI6.9_V_Asc		
Month	Min	Max	Mean	Min	Max	Mean	Min	Max	Mean	Min	Max	Mean
Jan	79.48	337.23	236.63	80.57	328.74	241.68	148.86	325.09	259.20	149.19	336.78	265.00
Feb	79.42	332.27	236.94	80.62	332.85	242.23	148.60	325.10	259.84	149.09	334.00	265.97
Mar	80.26	336.83	238.27	80.86	335.89	243.84	149.26	326.45	261.45	149.51	334.81	268.06
Apr	80.00	340.90	239.95	79.90	331.19	245.87	151.04	328.80	263.10	150.39	345.80	270.29
May	79.10	339.04	241.47	79.20	332.46	247.88	153.25	331.33	264.48	153.63	339.54	272.23
Jun	79.04	336.99	242.25	78.25	334.79	249.00	158.89	334.71	265.39	159.70	340.83	273.32
Jul	79.68	330.21	242.84	78.59	335.72	249.80	160.05	333.27	265.94	160.71	340.54	273.87
Aug	79.98	329.63	242.58	79.32	333.99	249.57	161.01	331.67	265.53	161.43	340.40	273.51
Sep	80.59	332.07	241.66	79.86	333.89	248.35	159.35	330.55	264.43	159.77	339.68	272.26
Oct	81.00	338.90	240.25	80.18	333.36	246.25	155.08	328.17	263.03	155.81	339.18	270.13
Nov	81.39	334.27	238.42	81.76	330.29	243.98	151.66	324.64	261.04	151.98	336.50	267.51
Dec	80.41	328.34	237.13	80.87	329.78	242.30	150.29	323.53	259.56	150.53	337.58	265.51

TABLE II
SAME AS TABLE I BUT FOR RST STANDARD DEVIATION ESTIMATIONS

	StD-TB6.9_H_Des			StD-TB6.9_H_Asc			StD-TBI6.9_V_Des			StD-TBI6.9_V_Asc		
Month	Min	Max	Mean	Min	Max	Mean	Min	Max	Mean	Min	Max	Mean
Jan	0.36	54.11	4.94	0.44	54.80	5.49	0.19	38.16	3.25	0.17	35.36	3.80
Feb	0.41	52.22	4.82	0.49	51.43	5.46	0.16	36.61	3.23	0.17	51.73	3.84
Mar	0.47	48.10	4.86	0.50	47.35	5.61	0.23	38.69	3.30	0.21	60.56	4.02
Apr	0.45	44.95	5.10	0.34	46.56	5.89	0.23	36.74	3.45	0.19	29.76	4.19
May	0.45	51.88	5.25	0.37	49.65	6.06	0.23	38.21	3.56	0.18	55.63	4.30
Jun	0.44	50.83	5.29	0.39	50.21	6.05	0.26	39.52	3.59	0.20	48.45	4.31
Jul	0.44	55.43	4.80	0.36	52.42	5.47	0.22	45.62	3.31	0.17	46.03	4.00
Aug	0.41	53.30	4.68	0.43	47.55	5.20	0.19	41.34	3.20	0.19	39.98	3.88
Sep	0.45	55.59	4.48	0.34	48.98	5.33	0.21	37.96	3.18	0.20	50.23	3.99
Oct	0.41	59.83	4.75	0.36	60.04	5.54	0.28	39.26	3.27	0.23	39.83	4.03
Nov	0.39	47.75	4.76	0.39	46.85	5.39	0.22	39.53	3.26	0.20	31.02	3.87
Dec	0.38	52.42	4.76	0.52	52.33	5.28	0.21	38.31	3.18	0.19	50.46	3.69

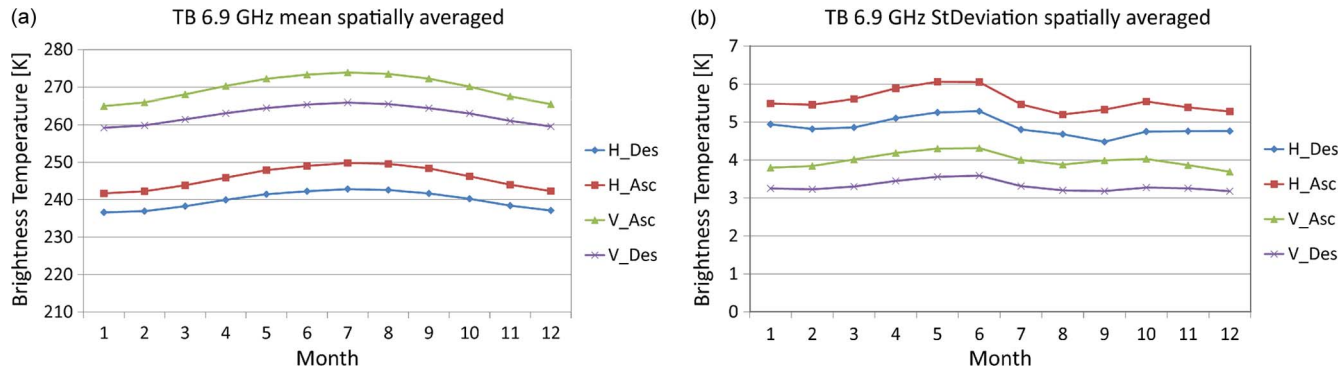

Fig. 1. Results of RST analysis on TB6.9, considering AMSR-E data from June 2002 to May 2011. (a) Annual trend of the spatial mean of the temporal means. (b) Annual trend of the spatial mean of the temporal standard deviations.

RST methodology should be able to significantly smooth such possible effects. Other possible interannual changes, due to RFI sources themselves, will be discussed later.

III. RESULTS

Once computed, the temporal means and the standard deviations of all the months of the year, to summarize the huge amount of the information arising from these reference fields (96 different information for each investigated signal), both the temporal reference fields (i.e., mean and standard deviation) have been spatially averaged over the whole global scene considering only land pixels, for each month of the year, using both polarizations (vertical and horizontal) and both orbit types (ascending and descending).

The summaries of the results obtained by analyzing TB6.9p are reported in Tables I and II in terms of the means and standard deviations, respectively, while Fig. 1 shows the yearly trends of the two signals. It should be stressed that such a procedure is affected by the larger number of land pixels at mid-North to North latitude with respect to the one from mid-South to South (the ratio is about 2.5); therefore, from a

climatological point of view, the results are more linked to northern climatology. The analysis of these first results allowed us several considerations: 1) Seasonal trends of TB6.9p are clearly evident, looking at the mean values [Fig. 1(a)], with an increase in temperature during summer in the Northern hemisphere; 2) as expected, TBs measured in vertical polarization are higher than those in the horizontal one; 3) TBs measured during ascending passes (i.e., 1:30 P.M. local time) are higher than those in nighttime due to the contribute of solar radiation; and 4) acquisitions in vertical polarization and during descending passes are the most stable [Fig. 1(b)]. Concerning this last achievement, owing to the scanning pattern of the sensor, the vertically polarized measurements are nearly always greater than the horizontal ones for all natural emissions, whether these are from natural or manmade surfaces. In addition, the range of variability of H data are larger than the V ones [9]. As a consequence, vertical acquisitions are more stable than the horizontal ones, which suffer also a greater influence of geophysical variability at the $\sim 55^{\circ}$ AMSR-E incidence angle [7]. Descending passes are acquired near 1:30 A.M. local time (thus, during nighttime), so it is reasonable to measure lower RFI than during ascending acquisitions because a minor human activity is likely to be in progress at that moment [5].

The evidence of RFI contamination in the measured signal is observable by looking at the maximum values of the mean and standard deviation reference fields; they respectively range between 323.53 K and 345.80 K and between 29.76 K and 60.56 K. Assuming a general land mean emissivity of 0.8 in the microwave, the effective land surface temperature should range between 404 K and 430 K, which are values well above the thermal emissive regime of natural Earth surfaces. Similar considerations can be done for standard deviation values that, as we stratified imagery in homogeneous datasets (i.e., monthly time window), are unlikely to be due to natural fluctuations. Therefore, such high values can be ascribable to anthropogenic sources.

Once the evidence of RFI contamination in the AMSR-E C-band has been assessed, the implementation of RST to the RI6.9p index, taking into account previous works [5], [7], [10], should allow for a better mapping of its presence. In addition to the aforementioned capability of the RI6.9p index to detect RFI presence, the multitemporal analysis we performed permitted the discrimination between the different temporal variability/persistence of RFI and naturally occurring geophysical processes. In Fig. 2, the RI6.9p annual behavior, in terms of the temporal mean and standard deviation at global scale, is shown. Looking first at Fig. 2(a), focusing on the RI6.9 mean value, the considerations already achieved by analyzing the TB6.9p signal are confirmed: A clear discrimination between data acquired at vertical and horizontal polarizations is evident, with the vertical measurements always higher than the horizontal ones. Such a behavior is established by also taking into account the different orbits of the sensor: Measurements achieved during descending passes are, in fact, higher than the ones during ascending passes. Moreover, in this case, a seasonal trend is recognizable, with a decrease in RI6.9 during summer, which may be related to the general minor ice coverage for the North hemisphere during this period. Considering the annual standard deviation

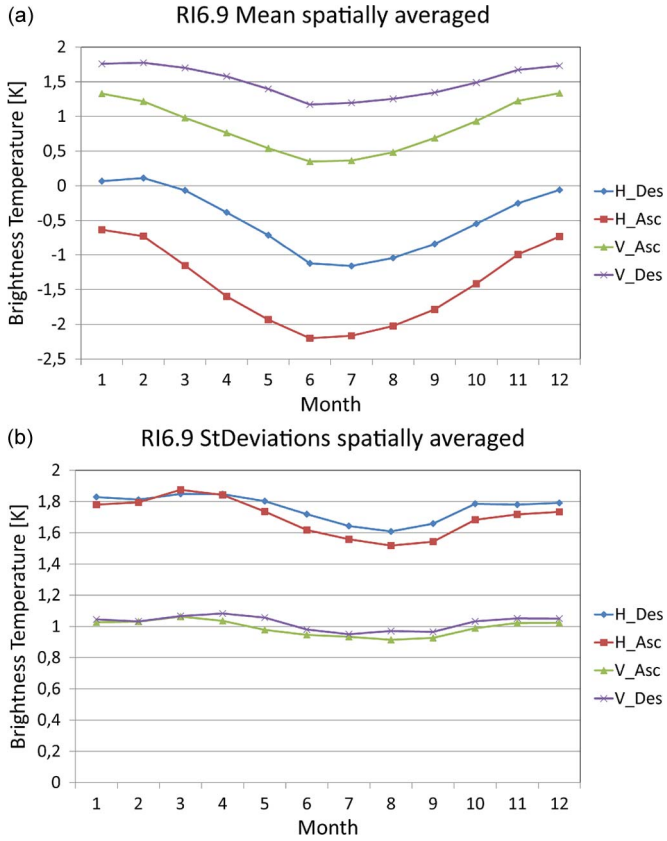

Fig. 2. Results of RST analysis on RI6.9, considering AMSR-E data from June 2002 to May 2011. (a) Annual trend of the spatial mean of the temporal means. (b) Annual trend of the spatial mean of the temporal standard deviations.

TABLE III
SUMMARY OF MONTHLY VALUES (IN KELVIN) OBTAINED BY AVERAGING OVER LAND PIXEL RI6.9P TEMPORAL STANDARD DEVIATION ESTIMATIONS ACHIEVED BY ANALYZING NINE YEARS OF AMSR-E C-BAND MEASUREMENTS

	StD-RI6.9_H_Des			StD-RI6.9_H_Asc			StD-RI6.9_V_Des			StD-RI6.9_V_Asc		
Month	Min	Max	Mean	Min	Max	Mean	Min	Max	Mean	Min	Max	Mean
Jan	0.23	49.99	1.83	0.17	47.95	1.78	0.16	39.98	1.04	0.14	30.34	1.03
Feb	0.21	43.43	1.81	0.20	43.89	1.79	0.15	38.45	1.03	0.13	52.00	1.03
Mar	0.22	40.64	1.85	0.22	41.16	1.88	0.18	41.09	1.07	0.14	61.79	1.06
Apr	0.23	39.36	1.85	0.20	42.22	1.84	0.18	38.43	1.08	0.15	31.54	1.04
May	0.22	36.45	1.80	0.19	44.21	1.74	0.16	38.50	1.06	0.14	56.81	0.98
Jun	0.23	40.16	1.72	0.19	42.15	1.62	0.15	38.72	0.98	0.14	49.23	0.95
Jul	0.23	45.89	1.64	0.20	39.85	1.56	0.16	38.49	0.95	0.16	47.16	0.93
Aug	0.23	47.63	1.61	0.21	39.26	1.52	0.16	42.67	0.97	0.16	33.92	0.91
Sep	0.21	40.87	1.66	0.20	39.35	1.54	0.15	39.62	0.97	0.15	51.29	0.93
Oct	0.22	44.67	1.79	0.21	43.68	1.68	0.16	36.13	1.03	0.14	39.68	0.99
Nov	0.23	40.80	1.78	0.20	42.33	1.72	0.20	41.87	1.05	0.16	30.72	1.02
Dec	0.23	48.96	1.79	0.21	43.01	1.73	0.19	39.86	1.05	0.18	51.36	1.02

trend [Fig. 2(b)], the previous achievements are confirmed too: Measurements acquired at vertical polarization and during descending passes are the most stable.

Once the general trends of both signals are determined, we decided to focus more on the standard deviation signal, because it is more stable than the mean one and therefore more suitable for a better discrimination of RFI [7]. In Table III, the summary of results achieved by the aforementioned analyses described for the standard deviation reference field (i.e., StD-RI6.9p) is reported. Again, the maximum, minimum, and globally averaged (i.e., mean) values are reported for each calendar month. The mean values of this signal, obtained by averaging all pixels

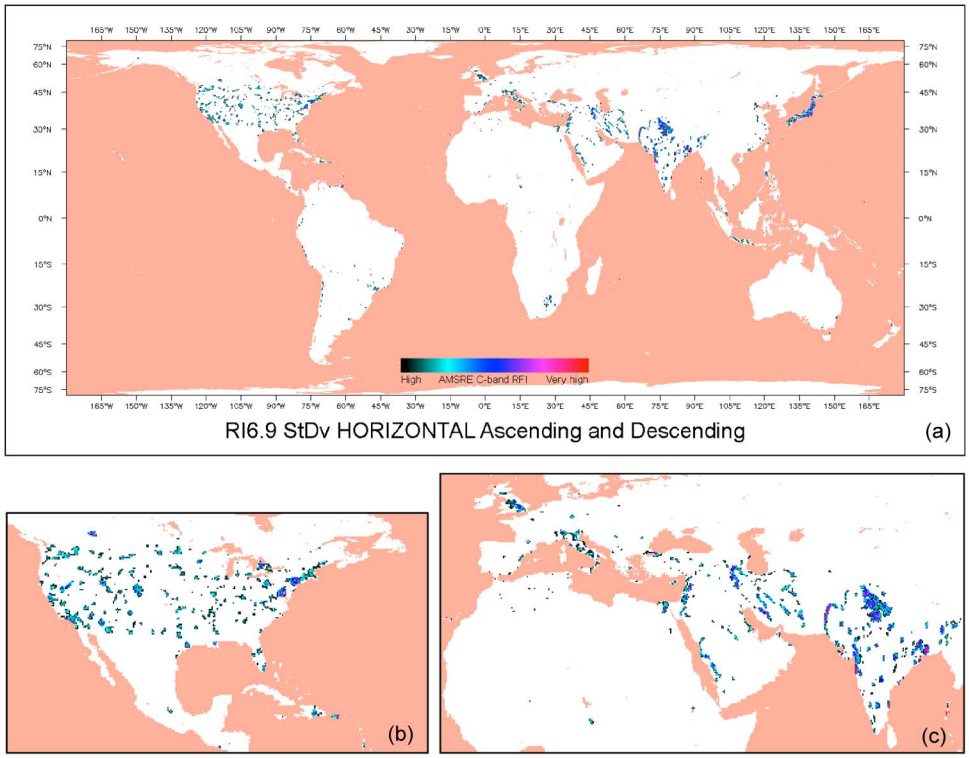

Fig. 3. AMSR-E C-band RFI source maps (high values). Only data acquired at horizontal polarization for both ascending and descending passes. (a) Global results. (b) Zoom over North America and (c) Europe and Asia. The color bar shows the whole range of RFI fluctuation over land.

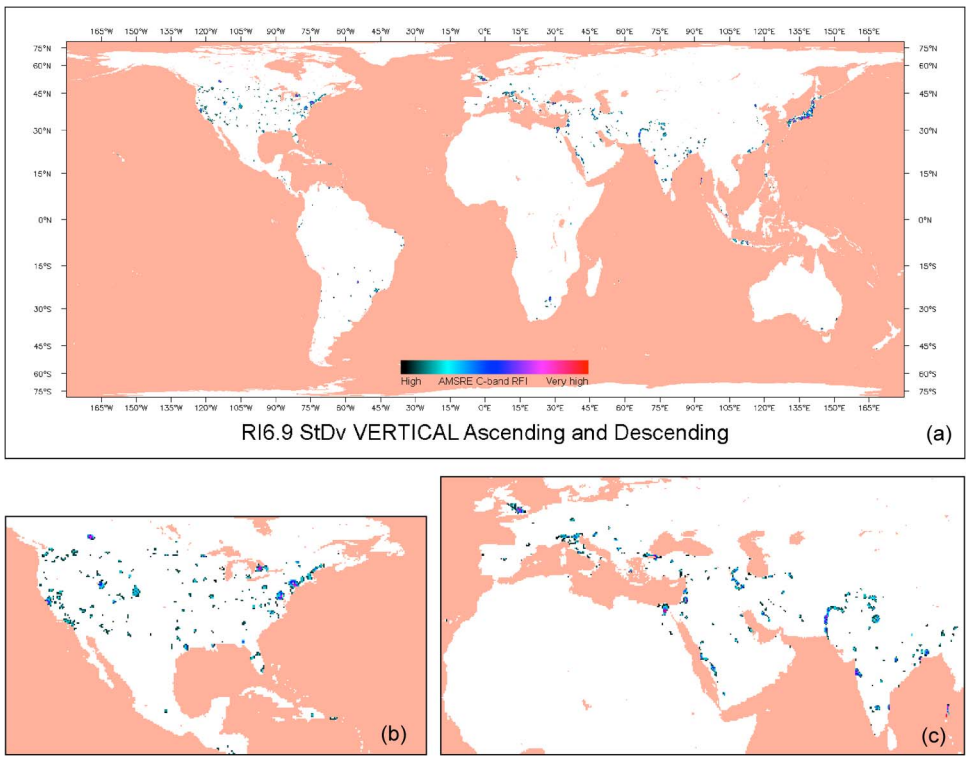

Fig. 4. Same as Fig. 3, considering only data acquired at vertical polarization for both ascending and descending passes. The color bar shows the whole range of RFI fluctuation over land.

at global scale, are between 0.91 K and 1.88 K. These values are likely to be very poorly affected by RFI perturbations, as the unperturbed points on the map are surely significantly more numerous than RFI sources, and thus should represent the expected values of the StD-RI6.9p signal in the absence of RFI.

On the other hand, maximum values of StD-RI6.9p, ranging between 30.34 K and 61.79 K, represent sure outliers of the distribution and can be associated to space–time anomalies whose persistence can allow us to discriminate anthropogenic (e.g., RFI) from natural causes.

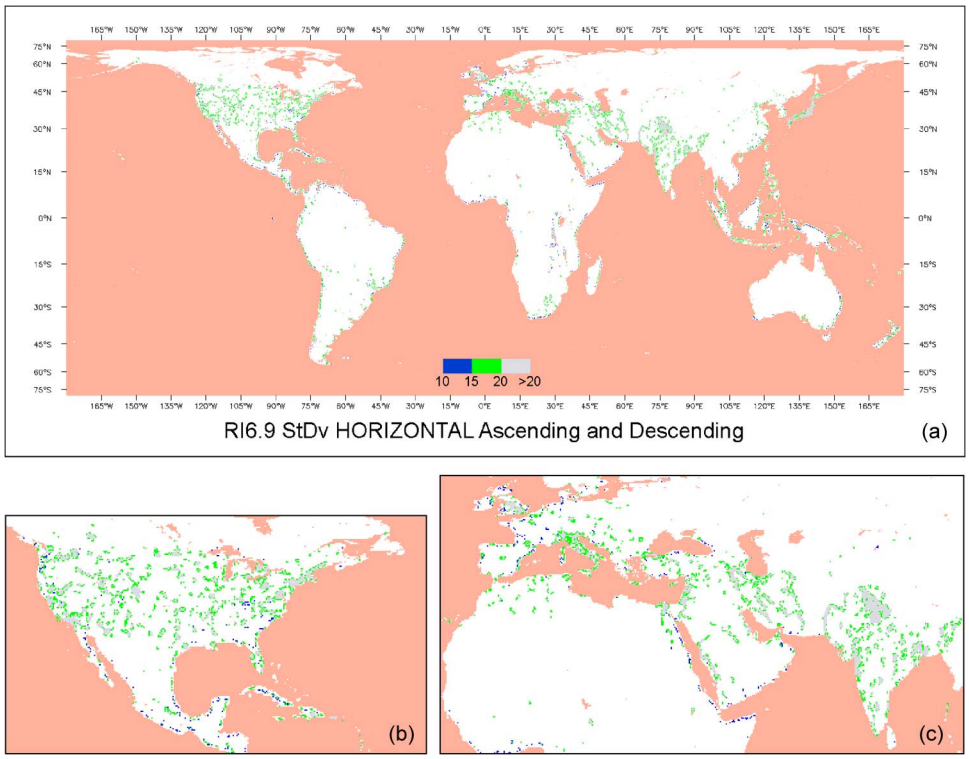

Fig. 5. AMSR-E C-band RFI source maps (low–medium values). Only data acquired at horizontal polarization for both ascending and descending passes. (a) Global results. (b) Zoom over North America and (c) Europe and Asia. The color bar shows the range of StDevRI6.9 (in kelvin) fluctuation over land.

Analyzing the statistical distribution of the 48 reference fields generated for the StD-RI6.9p signal, we found that, in all cases, more than 99% of values are less than 20 K (98% of them are less than 10 K); thus, we generated two AMSR-E C-band RFI source maps, identifying all those pixels characterized by high ($>$ 20 K) and persistent (for every month of the year) values of standard deviation, combining signals acquired at a specific polarization achieved for both ascending and descending passes (Figs. 3 and 4). Such an analysis intends to enhance all the areas that, worldwide, are affected by strong and persistent RFI.

Looking at these maps, first of all, it is possible to confirm the previous achievements: RFIs are more diffuse and intense for AMSR-E C-band data acquired at horizontal polarization. As expected, there is a good agreement between the localization of the areas affected by RFI in the two maps. Note that, in fact, a large part of North America seems to be RFI contaminated as well as several zones in India, South America, Japan, and Europe. These results, which mainly give information about the localization of areas with a high level of RFI, are in agreement with those already obtained in previous studies [5], [7]–[10].

Concerning result reliability and accuracy, the possible error sources are briefly mentioned here, assessing their possible impact on RFI maps. First, interannual changes of RFI sources should be discussed. These changes may occur if RFI sources appear/disappear in the nine-year period considered here (e.g., recent radio/TV transmitters absent in the first years of our spanning period or “old” RFI sources now switched off). This circumstance may have an impact on our RFI maps in terms of possible false negatives because, as described, we require temporal persistence to flag RFIs.

Finally, combining the information arising from the analysis we performed, we looked for the areas where possible weak RFI is present. The output of this study is shown in Figs. 5 and 6. To generate these maps, we looked at pixels characterized by StDevRI6.9 values between 10 K and 20 K at different threshold levels with 5 K steps (i.e., 10–15 K and 16–20 K), combining again signals acquired at a specific polarization for both ascending and descending passes. Therefore, the persistence is the driving feature of such an analysis, and the resulting maps show, in different colors according to the intensity of the index, only the areas presenting this persistence. All the inland areas (excluding those at very high latitudes) where such a persistence has been observed at StDevRI6.9 values lower than 10 K or where no persistence has been identified are depicted in white. Such areas should correspond to the zones with high natural geophysical variability (e.g., presence/absence of ice in different periods, high seasonal variability, etc.). Moreover, the previously identified strong RFI sources are masked in gray. Both Figs. 5 and 6 seem to indicate a residual presence of RFI sources, while large areas of the world should be free from signal effects like those due to RFI.

In detail, 5163 pixels show StDevRI6.9 values between 16 K and 20 K for the horizontal signal (green pixels in Fig. 5), almost the same number (i.e., 5210 pixels) of those already identified as strongly affected by RFI (i.e., $>$ 20, see Fig. 3 or the gray pixels in Fig. 5). Only 1078 pixels have been detected in the 10 K range (blue pixels in Fig. 5). For the vertical signal, 2742 pixels were strongly affected by RFI (Fig. 4 or gray pixels in Fig. 6), 2615 are those with StDevRI6.9 values between 16 K and 20 K (green pixels in Fig. 6), and 1021 are in the range of 10–15 K (blue pixels in Fig. 6). Such numbers first

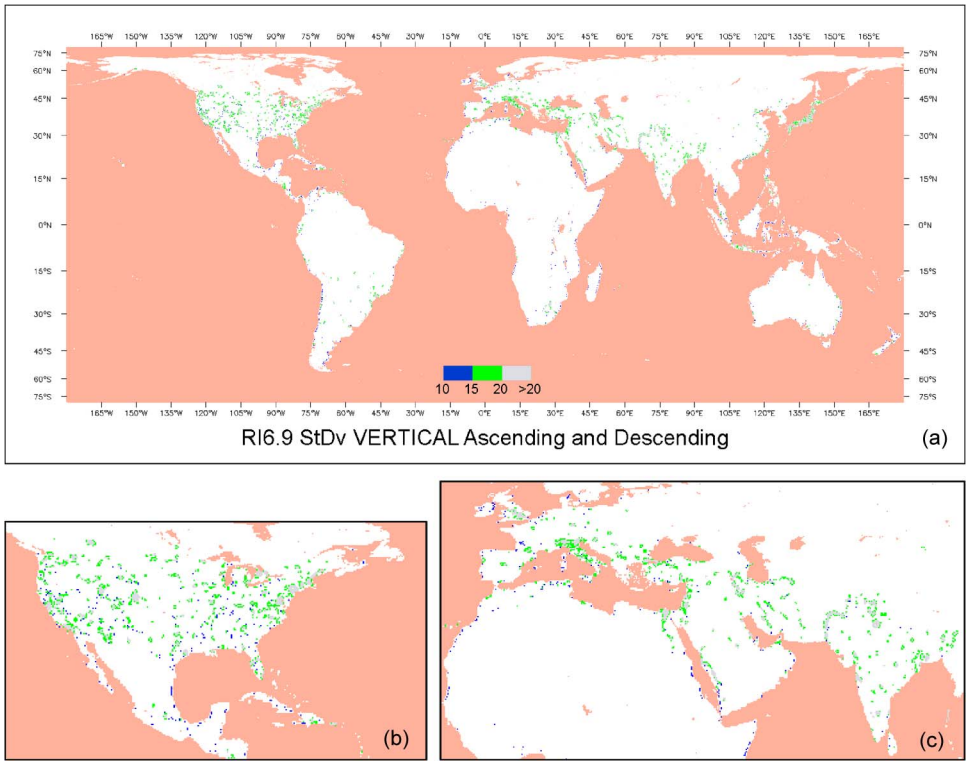

Fig. 6. Same as Fig. 5, considering only data acquired at vertical polarization for both ascending and descending passes. The color bar shows the range of StDevRI6.9 (in kelvin) fluctuation over land.

confirm that RFI at medium–high level (i.e., 16–20 K) are more diffuse and intense for AMSR-E C-band data acquired at horizontal polarization. These highly residual StDevRI6.9 values (green pixels) are mainly located in the areas next to the ones already detected as strongly affected by RFI, and so, it is reasonable to define them as possibly RFI contaminated. New possibly isolated RFI sources have been highlighted by such an analysis, particularly in Europe (e.g., France and Spain), even if they need to be confirmed by further studies also by using reliable *in situ* information. Low–medium levels of RFI (blue pixels) are instead more localized along coastlines, even if, also in this case, few isolated inland pixels have been detected. The coastline effect is due to the ocean emission by antenna side lobes [7], [10] and could be easily removed by using a coastline mask. Coming back to the amount of pixels detected at the different StDevRI6.9 thresholds, it is interesting to observe that, while the number of pixels identified at medium–high level (i.e., 5163 and 2615) seem to be related to the ones already obtained for high–strong values (i.e., 5210 and 2742), at both polarizations (H and V), the amounts of the pixels identified using StDevRI6.9 values in the 10–15 K range are very similar in both polarizations (i.e., 1078 and 1021) and, being more distributed along coastlines, are less dependent on the previously identified RFI sources. Such a result seems to indicate that the 10 K threshold could be effective in discriminating residual low-level RFI sources and natural geophysical variability. In any case, although these results deserve further analyses to be confirmed, a first indication about the global distribution of low–medium levels of RFI is clearly recognizable in such maps.

IV. Conclusion

RFI, contaminating signal measured by AMSR-E aboard the Aqua satellite mainly at C-bands, but also at X-bands, has been analyzed. Due to the lack of a reliable global ground truth, at least over land, and the difficulty in discriminating the weak level of RFI from natural geophysical variability, such a field of investigation still deserves more analyses. This is why, in this work, we tried to assess the potential of the RST approach for the identification of AMSR-E C-band RFI effects at global scale. RST, which is a multitemporal strategic analysis of satellite data, taking into account the historic variability at pixel level of the studied signal, can help in identifying high-level RFI-affected areas as well as in providing a first indication about areas where weak RFI signals are possibly present. Nine years of AMSR-E Level-3 land-surface products have been investigated, developing first two different maps, indicating, for data acquired at vertical and horizontal polarizations and for both ascending and descending passes, strong RFI occurrences. The achieved results, which generally appear in agreement with previous studies, have shown that the RFI effects seem to be more evident in data acquired at horizontal polarization during ascending passes.

In addition, a first attempt devoted to a better identification of areas affected by weak levels of RFI has been carried out, also trying to discriminate them from those characterized by natural variability due to geophysical and/or meteorological processes. The preliminary results seem to confirm the presence of the medium–high level of RFI in the areas close to the ones already identified as strongly affected by RFI, even if few isolated new sources have been detected also at low–medium values. These

results need to be further investigated to better understand the nature of these effects. To this scope, a validation of the obtained maps (at all levels) with *in situ* information will provide a confirmation of the reliability and accuracy of the achieved results. Considering that punctual information about RFI sources will be difficult to achieve, we will try to identify few large homogenous areas that are possibly RFI free (i.e. far from big cities, airports, etc.), assessing their behavior in terms of the RFI index we used in this work.

Owing to its independence on the investigated signal, the same approach used here will be extended to sea surfaces as well as to AMSR-E X- and K-band measurements to have a comprehensive view of RFI contamination on AMSR-E radiances even if, since October 2011, it is no longer operational. Anyway, such a study may be useful for other missions working at these wavelengths as well as in localizing where these data have to be used with attention in retrieving information about surface parameters.

REFERENCES

[1] J. R. Piepmeier, "RFI problems and solutions in spaceborne microwave radiometers," in *Proc. 29th URSI Gen. Assembly*, Chicago, IL, Aug. 7–16, 2008.

[2] A. J. Gasiewski, M. Klein, A. Yevgrafov, and V. Leuskiy, "Interference mitigation in passive microwave radiometry," in *Proc. IEEE Int. Geosci. Remote Sens. Symp.*, 2002, vol. 3, pp. 1682–1684.

[3] S. Misra, P. N. Mohammed, B. Güner, C. S. Ruf, J. R. Piepmeir, and J. T. Johnson, "Microwave radiometer radio-frequency interference detection algorithms: A comparative study," *IEEE Trans. Geosci. Remote Sens.*, vol. 47, no. 11, pp. 3742–3754, Nov. 2009.

[4] R. Oliva, E. Daganzo-Eusebio, Y. H. Kerr, S. Mecklenburg, S. Nieto, P. Richaume, and C. Gruhier, "SMOS Radio frequency interference scenario: Status and actions taken to improve the RFI environment in the 1400–1427-MHz passive band," *IEEE Trans. Geosci. Remote Sens.*, vol. 50, no. 5, pp. 1427–1439, May 2012.

[5] L. Li, E. G. Njok, E. Im, P. S. Chang, and K. St. Germain, "A preliminary survey of radio-frequency interference over the U.S. in Aqua AMSR-E data," *IEEE Trans. Geosci. Remote Sens.*, vol. 42, no. 2, pp. 380–390, Feb. 2004.

[6] L. Li, P. W. Gaiser, and M. Bettenhausen, "WindSat radio-frequency interference signature and its identification over land and ocean," *IEEE Trans. Geosci. Remote Sens.*, vol. 44, no. 3, pp. 530–539, Mar. 2006.

[7] E. G. Njoku, P. Ashcroft, T. K. Chan, and L. Li, "Global survey and statistics of radio-frequency interference in AMSR-E land observations," *IEEE Trans. Geosci. Remote Sens.*, vol. 43, no. 5, pp. 938–947, May 2005.

[8] S. W. Ellingson and J. T. Johnson, "A polarimetric survey of radio-frequency interference in C- and X-bands in the continental United States using WindSat radiometry," *IEEE Trans. Geosci. Remote Sens.*, vol. 44, no. 3, pp. 540–548, Mar. 2006.

[9] C. Kidd, "Radio frequency interference at passive microwave Earth observation frequencies," *Int. J. Remote Sens.*, vol. 27, no. 10, pp. 3853–3865, 2006.

[10] Y. Wu and F. Weng, "Detection and correction of AMSR-E radio-frequency interference," *Acta Meteorol. Sin.*, vol. 25, no. 5, pp. 669–681, 2011.

[11] ITU, Radio Regulations, Geneva, Switzerland: Int. Telecommun. Union, 2011.

[12] A. Camps, A. J. Gourrion, J. M. Tarongi, A. Gutiérrez, J. Barbosa, and R. Castro, "RFI analysis in SMOS imagery," in *Proc. IEEE IGARSS*, 2010, pp. 2007–2010.

[13] M. K. Hallikainen, J. Seppänen, A. Hakkarainen, and A. Rautiainen, "Studies of radio frequency interference at L-band using an airborne 2-D interferometric radiometer," in *Proc. IEEE Int. Geosci. Remote Sens. Symp.*, 2010, pp. 2490–2491.

[14] N. Skou, S. Misra, J. E. Balling, S. S. Kristensen, and S. S. Sobjaerg, "L-band RFI as experienced during airborne campaigns in preparation for SMOS," *IEEE Trans. Geosci. Remote Sens.*, vol. 48, pt. 2, no. 3, pp. 1398–1407, Mar. 2010.

[15] E. Anterrieu, "On the detection and quantification of RFI in L1a signals provided by SMOS," *IEEE Trans. Geosci. Remote Sens.*, vol. 49, pt. 2, no. 10, pp. 3986–3992, Oct. 2011.

[16] R. Castro, A. Gutiérrez, and J. Barbosa, "A first set of techniques to detect radio frequency interferences and mitigate their impact on SMOS data," *IEEE Trans. Geosci. Remote Sens.*, vol. 50, no. 5, pp. 1440–1447, May 2012.

[17] S. Mecklenburg, M. Drusch, Y. H. Kerr, J. Font, M. Martin-Neira, S. Delwart, G. Buenadicha, N. Reul, E. Daganzo-Eusebio, R. Oliva, and R. Crapolicchio, "ESA's soil moisture and ocean salinity mission: Mission performance and operations," *IEEE Trans. Geosci. Remote Sens.*, vol. 50, pt. 1, no. 5, pp. 1354–1366, May 2012.

[18] S. Misra and C. S. Ruf, "Analysis of radio frequency interference detection algorithms in the angular domain for SMOS," *IEEE Trans. Geosci. Remote Sens.*, vol. 50, no. 5, pp. 1448–1457, May 2012. doi:10.1109/TGRS.2011.2176949.

[19] B. Guner, J. T. Johnson, and N. Niamsuwan, "Time and frequency blanking for radio-frequency interference mitigation in microwave radiometry," *IEEE Trans. Geosci. Remote Sens.*, vol. 45, pt. 2, no. 11, pp. 3672–3679, Nov. 2007.

[20] M. Kachi, K. Imaoka, H. Fujii, A. Shibata, M. Kasahara, Y. Iida, N. Ito, K. Nakagawa, and H. Shimoda, "Status of GCOM-W1/AMSR2 development and science activities sensors, systems, and next-generation satellites XII," in *Proc. SPIE*, R. Meynart, S. P. Neeck, H. Shimoda, and S. Habib, Eds., 2008, vol. 7106, pp. 71060P-1–71060P-8.

[21] Japan Aerospace Exploration Agency (JAXA) Press Release, Launch Result of the Global Changing Observation Mission 1st—Water "SHIZUKU" (GCOM-W1) and the Korean Multi-purpose Satellite 3 (KOMPSAT-3) by H-IIA Launch Vehicle No. 21, 2012. [Online]. Available: http://www.jaxa.jp/press/2012/05/20120518_h2af21_e.html

[22] D. M. Le Vine, G. S. E. Lagerloef, F. R. Colomb, S. H. Yueh, and F. A. Pellerano, "Aquarius: An instrument to monitor sea surface salinity from space," *IEEE Trans. Geosci. Remote Sens.*, vol. 45, pt. 1, no. 7, pp. 2040–2050, Jul. 2007.

[23] S. Misra and C. S. Ruf, "Detection of radio-frequency interference for the aquarius radiometer," *IEEE Trans. Geosci. Remote Sens.*, vol. 46, pt. 2, no. 10, pp. 3123–3128, Oct. 2008.

[24] D. Entekhabi, E. G. Njoku, P. E. O'Neill, K. H. Kellogg, W. T. Crow, W. N. Edelstein, J. K. Entin, S. D. Goodman, T. J. Jackson, J. Johnson, J. Kimball, J. R. Piepmeier, R. D. Koster, N. Martin, K. C. McDonald, M. Moghaddam, S. Moran, R. Reichle, J. C. Shi, M. W. Spencer, S. W. Thurman, L. Tsang, and J. Van Zyl, "The soil moisture active passive (SMAP) mission," *Proc. IEEE*, vol. 98, no. 5, pp. 704–716, May 2010.

[25] J. R. Piepmeier, P. N. Mohammed, and J. J. Knuble, "A double detector for RFI mitigation in microwave radiometers," *IEEE Trans. Geosci. Remote Sens.*, vol. 46, no. 2, pp. 458–465, Feb. 2008.

[26] C. S. Ruf, S. M. Gross, and S. Misra, "RFI detection and mitigation for microwave radiometry with an agile digital detector," *IEEE Trans. Geosci. Remote Sens.*, vol. 44, no. 3, pp. 694–706, Mar. 2006.

[27] V. Tramutoli, "Robust Satellite Techniques (RST) for natural and environmental hazards monitoring and mitigation: Ten years of successful applications," in *Proc. 9th Int. Symp. Phys. Meas. Signatures Remote Sens.*, S. Liang, J. Liu, X. Li, R. Liu, and M. Schaepman, Eds., 2005, vol. 36, no. 7/W20, pp. 792–795, ISPRS: Beijing, China.

[28] V. Tramutoli, "Robust satellite techniques (RST) for natural and environmental hazards monitoring and mitigation: Theory and applications," in *Proc. MultiTemp*, 2007, pp. 1–6.

[29] T. Lacava, G. Calice, I. Coviello, N. Pergola, and V. Tramutoli, "Advanced multi-temporal passive microwave data analysis for soil wetness monitoring and flood risk forecast," in *Proc. IEEE Int. Geosci. Remote Sens. Symp.*, 2009, vol. 3, pp. 490–493.

[30] T. Lacava, I. Coviello, G. Mazzeo, N. Pergola, and V. Tramutoli, "On the potential of the AMSR-E based Polarization Ratio Variation Index (PRVI) for soil wetness variations monitoring," in *Proc. IEEE Int. Geosci. Remote Sens. Symp.*, 2010, pp. 4415–4418.

[31] M. Temimi, T. Lacava, T. Lakhankar, V. Tramutoli, H. Ghedira, and R. Khanbilvardi, "A multi-temporal analysis of AMSR-E data for flood and discharge monitoring during the 2008 flood in Iowa," *Hydrol. Process.*, vol. 25, no. 16, pp. 2623–2634, Jul. 2011.

[32] T. Lacava, I. Coviello, N. Pergola, and V. Tramutoli, "A RST-based study of AMSRE C-band radio frequency interferences," in *Proc. IEEE Int. Geosci. Remote Sens. Symp.*, 2010, pp. 2495–2498.

[33] E. G. Njoku, *AMSR-E/Aqua Daily L3 Surface Soil Moisture, Interpretive Parameters, & QC EASE-Grids V002 June 2002–May 2011*. Boulder, CO: Nat. Snow Ice Data Center, 2011.

Teodosio Lacava (M'11) was born in Potenza, Italy, in 1972. He received the M.S. degree in geological sciences and the Ph.D. degree in methods and technologies for environmental monitoring from the University of Basilicata, Potenza, in 1999 and 2004, respectively.

Since 2005, he has been a Researcher with the Institute of Methodologies for Environmental Analysis, Italian National Research Council (CNR), Tito Scalo, Potenza. His main interests are in the field of satellite data analysis for environmental research, particularly regarding the development and assessment of advanced satellite techniques for natural hazard investigation. In particular, his work is based on the analysis of high-temporal-resolution satellite data acquired both in the optical and microwave ranges of the electromagnetic spectrum. He has been a Coinvestigator of several European Union, Italian Space Agency, and CNR projects. He is the author of several peer-reviewed scientific journal articles. He also served as referee for many international journals.

Dr. Lacava is a member of the American Geophysical Union.

Irina Coviello was born in Potenza, Italy, in 1982. She received the M.S. degree in computer sciences from the University of Basilicata, Potenza, Italy, in 2006, where she is currently working toward the Ph.D. degree in environmental engineering, working on the development of an innovative system for storing and managing large volumes of satellite data.

Since 2006, she has been collaborating with the Institute of Methodologies for Environmental Analysis, National Research Council, Tito Scalo, Potenza. Her main interests are the study of methodologies and techniques for the analysis and processing of multitemporal satellite data for environmental research. In particular, she is responsible for the design and development of suitable software for the analysis of a long-term series of high-temporal-resolution satellite data. She is the author of several peer-reviewed scientific journal articles. She has also been a Coinvestigator of several European Union, Italian Space Agency, and CNR projects.

Mariapia Faruolo was born in Potenza, Italy, in 1980. She received the M.S. and Ph.D. degrees in environmental engineering from the University of Basilicata, Potenza, in 2006 and 2012, respectively.

Since 2007, she has been collaborating with the Institute of Methodologies for Environmental Analysis, National Research Council, Tito Scalo, Potenza. She is one of the researchers working for the Basilicata region Val d'Agri Environmental Observatory. Her main research activity is focused on the development of Robust Satellite Techniques for near-real-time detection and monitoring of flooded areas. In her study, she exploits data acquired both by optical and microwave sensors. She has been Coinvestigator of several Italian Space Agency, CNR, and European Union projects. She is also the author of several peer-reviewed scientific journal articles.

Giuseppe Mazzeo was born in Potenza, Italy, in 1977. He received the M.S. degree in environmental engineering and the Ph.D. degree in methods and technologies for environmental monitoring from the University of Basilicata, Potenza, in 2005 and 2008, respectively.

During 2009 and 2010, he was a Research Fellow with the University of Basilicata for the study of satellite thermal anomalies in fire-fighting operational context, and since 2011, he has been a Researcher with the Institute of Methodologies for Environmental Analysis, Italian National Research Council, Tito Scalo, Potenza. His main interests are in the field of satellite data analysis, particularly regarding the development and assessment of advanced techniques for natural hazard investigation by using high-temporal-resolution data (e.g., MSG-SEVIRI, EOS-MODIS, and NOAA-AVHRR). He is the author of several peer-reviewed scientific journal articles.

Nicola Pergola (M'10) received the M.S. degree in physics from the University of Rome "La Sapienza," Rome, Italy, on May 1993.

Since 1998, he has been a Researcher with the Institute of Methodologies for Environmental Analysis (IMAA), National Research Council (CNR), Tito Scalo, Potenza, Italy, where he leads the "Geohazards" Unit of the IMAA Satellite Remote Sensing Laboratory. He was member of the "core team" Geohazards within the Integrated Global Observing Strategy project, contributing to the definition of new global observational strategies for geohazard mitigation. He was a Scientific Coordinator for different Italian Space Agency and CNR projects and a Coinvestigator of several European Union and international (e.g., ESA, NATO, and INTAS) projects. He was recently involved in several FP6 and FP7 projects. His main interests are in the field of development of advanced satellite data analysis, particularly regarding high-temporal-resolution sensors like NOAA-AVHRR, EOS-MODIS, and MSG-SEVIRI for environmental research and applications. In particular, his research activity is mainly focused on the development of robust satellite techniques for natural hazard investigation from space and on multitemporal satellite data analysis in the space–time domain, particularly using infrared satellite radiances. He is the author of about 50 papers on ISI journals and more than 150 publications and proceedings with peer reviewing and international distribution. He also serves as a Referee for several relevant international journals and is an Associate Editor of the international scientific journal *Geomatics, Natural Hazards and Risks* (Taylor & Francis Ed).

Dr. Pergola is a member of the European Geosciences Union.

Valerio Tramutoli was born in December 28, 1957. He received the M.S. degree in physics from the University of Rome "La Sapienza," Rome, Italy.

Since 1990, he has been with the Department of Engineering and Physics of the Environment (DIFA), University of Basilicata, Potenza, Italy, as a Senior Researcher (since 1993) holding (since 1997) courses of Satellite Remote Sensing at the Faculties of Sciences and Engineering. Since 1991, he has been a Visiting Scientist at the main international centers involved in the Earth's observation by satellite, taking part in several international projects and initiatives of the main space agencies like ESA, NASA, NASDA, and the Italian Space Agency (ASI). He has been the National Coordinator of the SEISMASS Project (funded by ASI), and the PI, or person responsible for DIFA participation, to several international projects funded by NATO and EC in the framework of the Science for Peace, FP6-IST, FP6-INTAS, and FP6+FP7 GMES initiatives. Since 2010, he has been the Coordinator of the European Project PRE-EARTHQUAKES funded by EC in the framework of the FP7-GMES-Space Program. His research activity has been focused on the development of new satellite sensors and techniques for natural, environmental, and technological hazard monitoring and mitigation. In this context, in 1998, he proposed the original RAT (now, RST) change detection approach, which was successfully used in a large spectrum of applications. He has been among the few scientists invited to participate, since 2001, to the IGOS-Geohazard Core Team instructed (by the most important space agencies, CEOS, FAO, UNESCO, ICSU, etc.) to define the new observational strategies for geohazard mitigation for the next decade. He served as Referee for the most important journals in the field and as Project Evaluator for several funding agencies at the European and extra-European levels. Since 2009, he has been a member of the Editorial Board of the international journal *Geomatics, Natural Hazards and Risk*. He is the author or coauthor of more than 150 papers published on international journals, scientific books, and international conference proceedings. He has been the Chair, Cochair, Organizer, or invited Speaker in the most important international conferences (EGU, AGU, and IUGG). Since 2007, he has been a permanent member of the IUGG Inter-Association Working Group on Electromagnetic Studies of Earthquakes and Volcanoes.